Precursor Structural Influences on the Final ZnO Nanoparticle Morphology from a Novel Family of Structurally Characterized Zinc Alkoxy Alkyl Precursors

Timothy J. Boyle,* Scott D. Bunge, Nicholas L. Andrews, Laura E. Matzen, Katherine Sieg, Mark A. Rodriguez, and Thomas J. Headley

Sandia National Laboratories, Advanced Materials Laboratory, 1001 University Boulevard SE, Albuquerque, New Mexico 87106

Received April 13, 2004. Revised Manuscript Received June 7, 2004

We have synthesized a variety of structurally diverse "Zn(OR)(Et)(solv)" and "$Zn(OR)_2(solv)_2$" where Et = CH_2CH_3 and solv = no bound solvent, pyridine (py), tetrahydrofuran (THF), or 1-methyl imidazole (MeIm). The ligand OR represents the following: neo-pentoxide (ONep = OCH_2CMe_3), *tert*-butoxide ($OBu^t = OCMe_3$), cycloalkane-substituted methoxide [$(OCH_2\overline{C(CH_2)_n}$, $n = 2$, OCH_2Pr^c; $n = 3$, OCH_2Bu^c], cyclopentoxide [$O\overline{CH(CH_2)_4}$ = OPe^c], tetrahydrofurfurylalkoxide [$OCH_2\overline{CH(CH_2)_3O}$] = OTHF], and several aryloxides [OAr = 2,6-dimethyl phenoxide (DMP), 2,6-di-isopropyl phenoxide (DIP), and 2,6-di-*tert*-butyl phenoxide (DBP)]. These compounds were characterized by single-crystal X-ray diffraction as $[Zn(OR)(Et)(py)]_2$ [OR = ONep (**1**), OBu^t (**2**)], $[Zn(\mu_3\text{-ONep})(Et)]_4$ (**3**), $Zn[Zn_3(\mu_3\text{-}OCH_2Pr^c)_4(Et)_3]_2$ (**4**), $[Zn(\mu_3\text{-}OCH_2Bu^c)(Et)]_4$ (**5**), $[Zn(\mu_3\text{-}OPe^c)(Et)]_4$ (**6**), Zn(OAr)(Et)$(solv)_2$ where OAr = DMP: solv = py (**7**), DIP: solv = py (**8**), MeIm (**8a**); DBP: solv = py (**9**) and $[Zn(DBP)(\mu\text{-Et})]_2$ (**9a**), $Zn(OAr)_2(solv)_2$ where OAr = DMP: solv = py (**10**), MeIm (**10a**), py/MeIm (**10b**), DIP: solv = py (**11**), MeIm (**11a**), DBP: solv = py (**12**), MeIm (**12a**), $[Zn(\mu_3\text{-OTHF})(Et)]_4$ (**13**). The solution state behavior of these compounds was explored by multinuclear NMR spectroscopy. In an effort to determine the effect of nuclearity on the final nanoparticle morphology and size, four representative nuclearities mono- (**8**), di- (**1**), tetra- (**13**), and hepta- (**4**) nuclear were chosen and used to generate nanoparticles of ZnO. The mononuclear compound formed polydispersed spherical nanoparticles of wurtzite, whereas the nanoparticles generated from the other samples were nanorods. A relationship between the precursors central core and the final morphological properties of the nanorods was proffered to explain the variations noted.

Introduction

Zinc oxide (ZnO) has diverse applications, such as sensors, catalysts, varistors, surface acoustic wave devices, electrooptic devices, photo- and electroluminescent devices, and dental implants.[1,2] The wurtzite structure of ZnO allows for nonstoichiometric compositions containing excess zinc ($Zn_{1+x}O$) to be formed. This structure also makes these materials of particular interest for use in semiconductor applications.[1,2] Recently, nanoparticles of metal oxides have been the focus of a number of research efforts due to the unusual physical properties that are expected upon entering this size regime. To control and manipulate the morphology of nanoparticles, which will ultimately dictate the electrical and optical properties of the final devices, a fundamental understanding of the precursors' structural characteristics and how they affect the final material properties is necessary.

Metal alkoxides ($M(OR)_x$) have been found to be excellent precursors to ceramic materials for solution ("sol−gel") routes and metal-organic chemical vapor deposition (MOCVD) routes.[3−7] This is mainly due to their high solubility, low decomposition and crystallization temperatures, relative ease of modification, and commercial availability. These same attributes should make $M(OR)_x$ excellent precursors to nanoparticles. We consider desirable nanoparticle precursors to be volatile, cleanly decompose to the oxide, and readily crystallize in high boiling, coordinating solvents.[8] Several simple alkoxy-modified zinc alkyl compounds have been characterized,[1,2] including $[Zn(OR)(R)]_n$, that range from mono- to hexanuclear species depending on the func-

* To whom correspondence should be addressed. Phone: (505)272-7625. Fax: (505)272-7336. E-mail: tjboyle@Sandia.gov.

(1) Kingery, W. D. *Introduction to Ceramics*; John Wiley & Sons: New York, 1960.
(2) Du, Y.; Zhang, M.-S.; Hong, J.; Shen, Y.; Chen, Q.; Yin, Z. *Appl. Phys. A* **2003**, *76*, 171.
(3) Bradley, D. C.; Mehrotra, R. C.; Rothwell, I. P.; Singh, A. *Alkoxo and Aryloxo Derivatives of Metals*; Academic Press: San Diego, 2001.
(4) Bradley, D. C.; Mehrotra, R. C.; Gaur, D. P. *Metal Alkoxides*; Academic Press: New York, 1978.
(5) Turova, M. Y.; Turevskaya, E. P.; Kessler, V. G.; Yanovskaya, M. I. *The Chemistry of Metal Alkoxides*; Kluwer Academic Publishers: Boston, 2002.
(6) Hubert-Pfalzgraf, L. G. *New J. Chem.* **1987**, *11*, 663.
(7) Chandler, C. D.; Roger, C.; Hampden-Smith, M. J. *Chem. Rev.* **1993**, *93*, 1205.
(8) Bunge, S. D.; Boyle, T. J.; Headley, T. J. *Nano Lett.* **2003**, *3*, 901.

10.1021/cm0493997 CCC: $27.50
Published on Web 07/17/2004

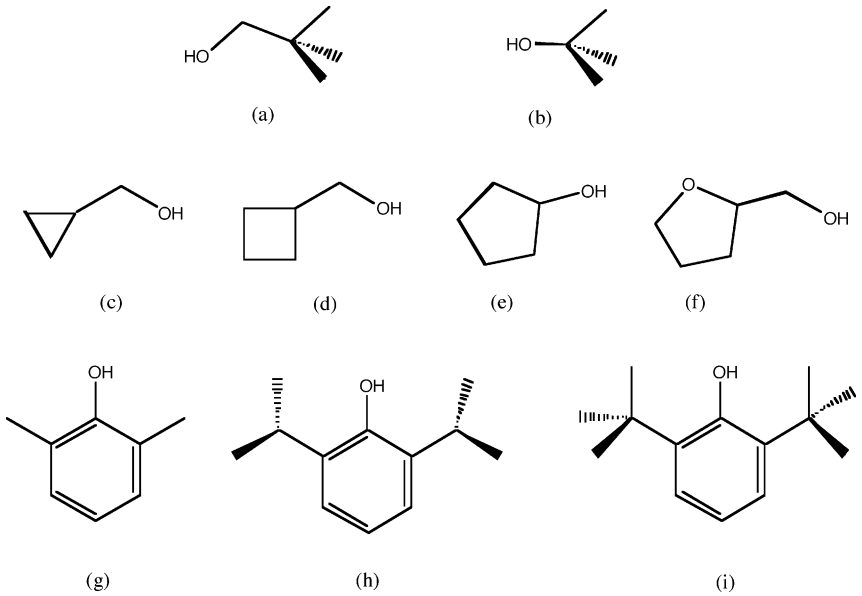

Figure 1. Schematic representation of ligands investigated: (a) H−ONep, (b) H−OBu^t, (c) H−OCH$_2$Pr^c, (d) H−OCH$_2$Bu^c, (e) H−OPe^c, (f) H−OTHF, (g) H−DMP, (h) H−DIP, and (i) H−DBP.

tionalization of the pendant ligand and [Zn(OR)$_2$(solv)]$_n$, that range from monomers to dimers depending on the presence of solvent. The solvents investigated are typically strong Lewis bases that minimize oligomerization due to the large size to charge ratio. In general, for these compounds, cubes, dimers, and monomers are reported with tetrahedrally (T_d) bound Zn metal centers. Despite this wide array of available zinc alkoxy and alkyl alkoxy precursors, we are not aware of any structurally characterized "Zn(OR)(R)" used to generate ZnO nanoparticles. While numerous reports utilize diethyl zinc ($ZnEt_2$) to synthesize nanoparticles, most do not modify this precursor. Of these investigations, only Carnes and Klabunde[9] used alcohols as the modifying agent. The process involved the modification of $ZnEt_2$ in situ with water, *tert*-butyl alcohol, and ethanol to generate 3−5-nm ZnO nanoparticles that aggregated to form larger particles. However, the resulting Zn intermediate was never characterized.

Due to the limited number of compounds with the desired characteristics and the dearth of investigations utilizing zinc alkoxy alkyls, we undertook the synthesis of a series of structurally diverse Zn(OR)(Et)(solv) and Zn(OR)$_2$(solv)$_2$ where Et = CH_2CH_3, solv = pyridine (py), tetrahydrofuran (THF), or methyl imidazole (MeIm), the ligand OR represented *neo*-pentoxide (ONep = OCH_2-CMe_3), *tert*-butoxide (OBu^t = $OCMe_3$), cycloalkane-substituted methoxide [$(OCH_2C(CH_2)_n$, $n = 2$, OCH_2Pr^c; $n = 3$, OCH_2Bu^c], cyclopentoxide [$OCH(CH_2)_4$ = OPe^c], tetrahydrofurfurylalkoxide [$OCH_2CH(CH_2)_3O$] = OTHF], and several aryloxides [OAr = 2,6-dimethyl phenoxide (DMP), 2,6-di-isopropyl phenoxide (DIP), 2,6-di-*tert*-butyl phenoxide (DBP)]. A schematic representation of these alcohols is shown in Figure 1.

These compounds were characterized by single-crystal X-ray diffraction as [Zn(OR)(Et)(py)]$_2$ [OR = ONep (**1**), OBu^t (**2**)], [Zn(μ_3-ONep)(Et)]$_4$ (**3**), Zn[Zn$_3$(μ_3-OCH$_2$Pr^c)$_4$-(Et)$_3$]$_2$ (**4**), [Zn(μ_3-OCH$_2$Bu^c)(Et)]$_4$ (**5**), [Zn(μ_3-OPe^c)(Et)]$_4$ (**6**), Zn(OAr)(Et)(solv)$_2$ where OAr = DMP: solv = py (**7**); DIP: solv = py (**8**), MeIm (**8a**); DBP: solv = py (**9**), and [Zn(DBP)(μ-Et)]$_2$ (**9a**), Zn(OAr)$_2$(solv)$_2$ where OAr = DMP: solv = py (**10**), MeIm (**10a**), py/MeIm (**10b**), DIP: solv = py (**11**), MeIm (**11a**)., DBP: solv = py (**12**), MeIm (**12a**), [Zn(μ_3-OTHF)(Et)]$_4$ (**13**). Selected structural geometries and ligands are represented by the thermal ellipsoid plots of **1**−**6**, **8**, **9a**, and **13** in Figures 2−10, respectively. Full experimental data for the remaining compounds is presented in the Supporting Information.

Representative "Zn(OR)(Et)(solv)" complexes of various nuclearities (**1**, **4**, **8**, and **13**) were used to generate nanoparticles from a novel route utilizing MeIm/H_2O. This paper discusses the synthesis and characterization of these compounds as well as the effect various precursor structures have on the growth of ZnO nanoparticles as determined by transmission electron microscopy (TEM).

Experimental Section

All compounds described below were handled with rigorous exclusion of air and water using standard Schlenk line and glovebox techniques. All solvents were stored under argon and used as received (Aldrich) in sure seal bottles, including hexanes (hex), toluene (tol), tetrahydrofuran (THF), pyridine (py), and 1-methylimidazole (MeIm). The following chemicals were used as received (Aldrich): $ZnEt_2$ (1.0 M in hexanes), H−ONep, HOBu^t, H−OTHF, H−OCH$_2$Pr^c, H−OCH$_2$Bu^c, H−OPe^c, H−DMP, H−DIP, and H−DBP (Figure 1).

FT-IR data were obtained on a Bruker Vector 22 Instrument using KBr pellets under an atmosphere of flowing nitrogen. Elemental analysis was performed on a Perkin-Elmer 2400 CHN-S/O elemental analyzer. All NMR samples were prepared from dried crystalline materials that were handled and stored under an argon atmosphere and redissolved in the appropriate deuterated solvent (benzene-d_6, toluene-d_8, THF-d_8, pyridine-d_5) at saturated solution concentrations. All solution spectra were obtained on a Bruker DRX400 spectrometer at 399.8 and 100.5 MHz for ^{1}H and ^{13}C experiments, respectively. A 5-mm broadband probe was used for all experiments. ^{1}H NMR spectra were obtained using a direct single-pulse excitation, with a 10-s recycle delay and 8-scan average. The ^{13}C{^{1}H} NMR spectra were obtained using a WALTZ-16 composite

(9) Carnes, C. L.; Klabunde, K. J. *Langmuir* **2000**, *116*, 3764.

pulse ^{1}H decoupling, a 5-s recycle delay, and a $\pi/4$ pulse excitation.

General Synthesis. After the appropriate alcohol was dissolved in the desired solvent, the reaction mixture was slowly added to a vial with $ZnEt_2$ in hexanes. The reactions involving MeIm included a stoichiometric addition of MeIm in toluene to the initial alcohol/solvent solution prior to addition to $ZnEt_2$ in hexanes. Upon addition, the reaction bubbled vigorously. Once this had subsided, the reaction mixture was allowed to stir for 12 h. After this time, the mixture was concentrated by rotary evaporation and either transferred to a freezer (−37 °C) or allowed to sit uncapped in the glovebox until crystals formed (<10 days).

[Zn(μ-ONep)(Et)(py)]$_2$ (1). Used H−ONep (0.133 g, 1.51 mmol), $ZnEt_2$ (1.50 mL, 1.50 mmol), and ∼5 mL of py. Yield: 0.600 g (76.7%). FT-IR (KBr, cm^{-1}): 2952(s), 2896(s), 2860(s), 2694(w), 1601(m), 1475(m), 1446(m), 1400(m), 1363(m), 1215(w), 1152(w), 1084(s), 1069(s), 1036(s), 1005(s), 752(m), 699(m), 561(m). ^{1}H NMR (399.872 Hz, py-d_5): δ 8.74 (2.0H, d, NC_5H_5, J_{H-H} = 1.0 Hz), 7.58 (1.0H, t, NC_5H_5, J_{H-H} = 3.4 Hz), 7.22 (2.0H, t, NC_5H_5, J_{H-H} = 3.1 Hz), 3.53 (2.0H, s, OCH_2CMe_3), 1.77 (2.0H, t, CH_2CH_3, J_{H-H} = 4.1 Hz), 0.88 (9.0H, s, OCH_2CMe_3), 0.75 (3.0H, q, CH_2CH_3, J_{H-H} = 4.0 Hz). Elemental analysis for $C_{12}H_{21}NOZn$: Calcd, 55.29% C, 8.12% H, 5.37% N. Found, 56.17% C, 7.79% H, 6.00% N.

[Zn(μ-OBu^t)(Et)(py)]$_2$ (2). Used H−OBu^t (2.00 g, 27.0 mmol), $ZnEt_2$ (27.0 mL, 27.0 mmol), and ∼25 mL of py. Yield: 6.01 g (90.1%). FT-IR (KBr, cm^{-1}): 2972(s), 2948(s), 2932(s), 2890(s), 2862(s), 2806(w), 1388(m), 1366(s), 1243(m), 1177(s), 902(s), 756(m), 611(m), 541(s), 463(m). Elemental Analysis for $C_{11}H_{19}NOZn$: Calcd, 53.56%C, 7.76%H, 5.68%N. Found 47.79%C, 7.24%H, 3.60%N.

[Zn(μ_3-ONep)(Et)]$_4$ (3). Used H−ONep (0.50 g, 5.68 mmol), $ZnEt_2$ (6.75 mL, 5.68 mmol), and ∼5 mL of hexanes. Yield: 0.500 g (48.5%). FT-IR (KBr, cm^{-1}): 2972(s), 2949(s), 2932(s), 2889(s) 2862(s), 2806(w), 1388(m), 1365(s), 1243(m), 1177(s), 902(s), 756(m), 611(m), 541(s), 463(m). Elemental analysis for $C_{28}H_{64}O_4Zn_4$: Calcd, 46.30% C, 8.88% H. Found, 46.48% C, 8.74% H.

Zn[Zn$_3$(μ_3-OCH$_2$Pr^c)$_3$(μ_3-OCH$_2$Pr^c)(Et)$_3$]$_2$ (4). Used H−OCH$_2$Pr^c (0.216 g, 3.00 mmol), $ZnEt_2$ (3.00 mL, 3.00 mmol), and ∼10 mL of hexanes. Yield: 2.89 g (81.3%). FT-IR (KBr, cm^{-1}): 3083(m), 3007(m), 2944(s), 2888(s), 2807(s), 1464(w), 1429(w), 1396(s), 1048(w), 1028(s), 999(s), 958(m), 925(m), 900(m), 830(m), 614(s), 551(s), 531(s), 506(s). ^{1}H NMR (399.8 MHz, C_6D_6): δ 3.84 (12.0H, d, $OCH_2\overline{CHCH_2CH_2}$), 3.69 (4.0H, d, $OCH_2\overline{CHCH_2CH_2}$), 1.49 (18.0H, t, CH_2CH_3), 1.28 (6.0H, m, $OCH_2\overline{CHCH_2CH_2}$)), 1.12 (2.0H, m, $OCH_2\overline{CHCH_2CH_2}$)), 0.60 (12.0H, m, CH_2CH_3), 0.56 (12.0H, m, $OCH_2\overline{CHCH_2CH_2}$)), 0.53 (4.0H, m, $OCH_2CHCH_2CH_2$), 0.39 (12.0H, m, $OCH_2CHCH_2\overline{CH_2}$)), 0.21 (4.0H, m, $OCH_2\overline{CHCH_2CH_2}$)). Elemental analysis for $C_{48}H_{86}O_8Zn_7$: Calcd, 44.01% C, 7.17% H. Found, 44.11% C, 6.65% H.

[Zn(μ_3-OCH$_2$Bu^c)(Et)]$_4$ (5). Used H−OCH$_2$Bu^c (0.262 g, 3.04 mmol), $ZnEt_2$ (3.00 mL, 3.00 mmol), and ∼10 mL of hexanes. Yield: 1.62 g (74.9%). FT-IR (KBr, cm^{-1}): 2977(s), 2931(s), 2856(s), 2806(w), 1380(m), 1332(w), 1242(w), 1155(w), 1104(q), 1049(m), 1003(s), 956(w), 921(w), 643(w), 612(m), 516(m), 486(m). ^{1}H NMR (399.8 MHz, C_6D_6): δ 3.83 (2.0H, d, $OCH_2\overline{CHCH_2CH_2CH_2}$), 2.59 (1.0H, m, $OCH_2\overline{CHCH_2CH_2}$), 2.05 (2.0H, m, $OCH_2\overline{CHCH_2CH_2CH_2}$)), 1.81 (2.0H, m, $OCH_2\overline{CHCH_2CH_2CH_2}$)), 1.64 (2.0H, m, $OCH_2\overline{CHCH_2CH_2}$), 1.59 (3.0H, m, CH_2CH_3), 0.66 (2.0H, q, CH_2CH_3). Elemental analysis for $C_{28}H_{56}O_4Zn_4$: Calcd, 46.82% C, 7.86% H. Found, 46.08% C, 7.60% H.

[Zn(μ_3-OPe^c)(Et)]$_4$ (6). Used H−OPe^c (0.258 g, 3.00 mmol), $ZnEt_2$ (3.00 mL, 3.00 mmol), and ∼10 mL of hexanes. Yield: 1.46 g (67.2%). FT-IR (Nujol, cm^{-1}): 2963(s), 2905(s), 2861(s), 2806(w), 1601(w), 1445(w), 1413(m), 1360(w), 1260(s), 1091(s), 1020(s), 799(w, sh), 702(w), 664(m), 613(m), 515(m). ^{1}H NMR (399.8 MHz, C_6D_6): δ 4.31 (1.0H, m, $OC\overline{HCH_2CH_2CH_2CH_2}$), 2.07 (2.0H, m, $OCH\overline{CH_2CH_2CH_2CH_2}$), 1.66 (2.0H, m, $OCH\overline{CH_2CH_2CH_2CH_2}$), 1.54 (3.0H, t, CH_2CH_3), 1.38 (4.0H, m, $OCH\overline{CH_2CH_2CH_2CH_2}$), 0.58 (2.0H, q, CH_2CH_3). Elemental analysis for $C_{28}H_{56}O_4Zn_4$: Calcd, 46.83% C, 7.86% H. Found, 47.20% C, 7.44% H.

Zn(DIP)(Et)(py)$_2$ (8). Used H−DIP (0.615 g, 3.45 mmol), $ZnEt_2$ (4.00 mL, 4.00 mmol), and ∼10 mL of py. Yield: 1.41 g (70.5%). FT-IR (KBr, cm^{-1}): 2969(s), 2959(s), 2921(m), 2843(m), 1601(s), 1585(sh, w), 1447(s), 1428(s), 1357(sh, w), 1338(m), 1282(m), 1259(m), 1212(m), 1069(m), 1038(s), 1011(m), 852(m), 751(s), 704(s), 594(w). Elemental analysis for $C_{19}H_{27}ONZn$: Calcd, 65.05% C, 7.76% H, 3.99% N. Found, 65.93% C, 7.23% H, 6.84% N.

[Zn(μ-DBP)(Et)]$_2$ (9a). Used H−DBP (0.651 g, 3.15 mmol), $ZnEt_2$ (3.15 mL, 3.15 mmol), and 10 mL of tol. Yield: 0.49 g (24.7%). FT-IR (KBr, cm^{-1}) 3002(sh, m), 2973(sh, s), 2955(s), 2862(m), 1482(m), 1465(m), 1427(sh, m), 1404(s), 1386(sh, m), 1350(m), 1264(m), 1231(sh, m), 1206(sh, m), 1185(s), 1119(m), 846(m), 807(m), 751(m), 622(m), 526(w). Elemental analysis for $C_{32}H_{52}O_2Zn_2$: Calcd, 64.11% C, 8.74% H. Found: 64.37% C, 8.75% H.

[Zn(μ_3-OTHF)(Et)]$_4$ (13). Used H−OTHF (0.30 g, 3.00 mmol), $ZnEt_2$ (3.00 mL, 3.00 mmol), and ∼10 mL of hexanes. Yield: 2.63 g (73.1%). FT-IR (KBr, cm^{-1}): 2963(s), 1605(w), 1413(sh, s), 1404(s), 1260(s), 1271(s), 1265(sh, s), 1237(m), 1090(s), 1020(s), 858(m), 701(s), 612(w), 513(w). ^{1}H NMR (399.8 MHz, C_6D_6): δ 4.18 (4.0H, m, $OCH_2\overline{CHCH_2CH_2CH_2O}$), 3.94 (4.0H, m, $OCH_2\overline{CHCH_2CH_2CH_2O}$), 3.72 (8.0H, m, $OCH_2\overline{CHCH_2CH_2CH_2O}$), 1.81 (4.0H, m, $OCH_2\overline{CHCH_2CH_2CH_2O}$), 1.69 (12.0H, m, CH_2CH_3), 1.43 (16.0H, m, $OCH_2\overline{CHCH_2CH_2CH_2O}$), 0.72 (8.0H, m, CH_2CH_3). Elemental analysis for $C_{28}H_{56}O_8Zn_4$: Calcd, 42.99% C, 7.22% H. Found, 42.30% C, 6.77% H.

Nanoparticle Synthesis. A 0.125 M py solution based on Zn of the appropriate precursor (**1**, **4**, **8**, and **13**) was rapidly introduced via syringe to a 25-mL Schlenk flask that contained MeIm/H_2O (9.50 mL/0.50 mL) heated to reflux temperatures. After 30 min, the heat was removed and the reaction allowed to cool to room temperature while stirring for an additional 12 h. Nanoparticles were isolated via centrifugation.

Transmission Electron Microscopy. An aliquot of the desired precipitate suspended in hexanes was placed directly onto a carbon-coated copper transmission electron microscopy (TEM) grid (300 mesh) purchased from Electron Microscopy Sciences. The aliquot was then allowed to dry. The resultant particles were studied using a Philips CM 30 TEM operating at 300-kV accelerating voltage.

Powder X-ray Diffraction. The powder X-ray diffraction (XRD) patterns of the ZnO nanocrystals were obtained on a Siemens 5D500 diffractometer using Cu Kα radiation, excited at 40 kV and 30 mA. The X-rays were collimated at the source with 1° divergence scatter slits with a detector that had 1° scatter and receiving slits using a graphite diffracted beam monochromator.

General X-ray Crystal Structure Information.[10] Each crystal was mounted onto a thin glass fiber from a pool of Fluorolube and immediately placed under a liquid N_2 stream, on a Bruker AXS diffractometer. The radiation used was graphite monochromatized Mo Kα radiation (λ = 0.7107 Å). The lattice parameters were optimized from a least-squares calculation on carefully centered reflections. Lattice determination and data collection were carried out using SMART Version 5.054 software. Data reduction was performed using SAINT Version 6.01 software. The structure refinement was performed using XSHELL 3.0 software. The data were cor-

(10) The listed versions of SAINT, SMART, XSHELL, and SADABS Software from Bruker Analytical X-Ray Systems Inc., 6300 Enterprise Lane, Madison, WI 53719, were used in analysis.

Table 1. Data Collection Parameters for 1−3

	compound		
	1	**2**	**3**
chemical formula	$C_{24}H_{42}N_2O_2Zn_2$	$C_{22}H_{38}N_2O_2Zn_2$	$C_{28}H_{64}O_4Zn_4$
formula weight	521.34	493.28	726.27
temp (K)	168	168	168(2)
space group	monoclinic *P*2(1)/*c*	monoclinic *P*2(1)/*c*	tetragonal *P*4(2)/*n*
a (Å)	10.0364(6)	9.0356(12)	12.8441(12)
b (Å)	19.0397(11)	16.287(2)	12.8441(12)
c (Å)	14.6644(9)	9.0483(12)	10.4873(19)
β (deg)	98.081(4)	110.124(2)	
V (Å^3)	2773.6(3)	1250.3(3)	1730.1(4)
Z	4	2	2
D_{calcd} (Mg/m^3)	1.248	1.310	1.394
μ (Mo Kα) (mm^{-1})	1.749	1.936	2.767
R1[a] (%) (all data)	3.63(4.63)	3.70 (4.71)	2.93 (3.95)
wR2[b] (%) (all data)	8.99 (9.54)	8.45 (8.86)	6.49 (6.88)

[a] $R1 = \sum||F_o| - |F_c||/\sum|F_o| \times 100$. [b] $wR2 = [\sum w(F_o^2 - F_c^2)^2/\sum(w|F_o|^2)^2]^{1/2} \times 100$.

Table 2. Data Collection Parameters for 4−6

	compound		
	4	**5**	**6**
chemical formula	$C_{44}H_{58}O_8Zn_7$	$C_{28}H_{56}O_4Zn_4$	$C_{28}H_{56}O_4Zn_4$
formula weight	1172.49	718.21	718.21
temp (K)	168(2)	168(2)	168(2)
space group	monoclinic *P*2(1)/*n*	tetragonal *I*4(1)/*a*	monoclinic *P*2(1)
a (Å)	11.6679(2)	16.994(4)	8.166(3)
b (Å)	19.309(3)	16.994(4)	19.155(8)
c (Å)	11.872(2)	11.133(3)	10.522(4)
β (deg)	97.432(3)		97.350(6)
V (Å^3)	2652.0(8)	3215.3(15)	1632.4(11)
Z	2	4	2
D_{calcd} (Mg/m^3)	1.486	1.484	1.461
μ (Mo Kα) (mm^{-1})	3.155	2.977	2.931
R1[a] (%) (all data)	3.77 (4.95)	2.77 (3.72)	4.81 (7.58)
wR2[b] (%) (all data)	10.31 (11.34)	6.24 (6.65)	10.02 (11.19)

[a] $R1 = \sum||F_o| - |F_c||/\sum|F_o| \times 100$. [b] $wR2 = [\sum w(F_o^2 - F_c^2)^2/\sum(w|F_o|^2)^2]^{1/2} \times 100$.

rected for absorption using the SADABS program within the SAINT software package.

Each structure was solved using direct methods. This procedure yielded the heavy atoms, along with a number of the C, N, and O atoms. Subsequent Fourier synthesis yielded the remaining atom positions. The hydrogen atoms were fixed in positions of ideal geometry and refined within the XSHELL software. These idealized hydrogen atoms had their isotropic temperature factors fixed at 1.2 or 1.5 times the equivalent isotropic U of the C atoms to which they were bonded. The final refinement of each compound included anisotropic thermal parameters on all non-hydrogen atoms. Hydrogen atoms were left off any disordered alkoxide ligands; however, the correct number of H atoms was entered in the final refinement to calculate proper values in the summary Tables 1−6. Additional information concerning the data collection and final structural solutions of **1**−**13** can be found in the Supporting Information. Any variations from standard structural solution associated with the representative compounds are discussed below.

Compound 4. Two of the alkoxide ligands, one bound to O(1) and the other bound to O(3), appeared to be disordered. The disorder flips the alkoxide ligand over two possible orientations and thereby disorders the C(2) carbon of the O(1) ligand over two positions C(2) and C(2′). Likewise, the C(10) carbon is disordered over two sites C(10) and C(10′) in the O(3) (Tri) ligand. Bond length restraints were used to improve the bond lengths of the disordered carbon atoms in the alkoxide ligands ($\sigma = 0.04$ Å). Hydrogens were calculated for the other well-behaved alkoxide and ethyl ligands.

Compound 13. Significant disordering of the alkoxide and ethyl ligands resulted in all atoms, with the exception of Zn(1) and O(1), being refined with only isotropic temperature

Table 3. Data Collection Parameters for 7, 8, and 8a

	compound		
	7	**8**	**8a**
chemical formula	$C_{15}H_{19}NOZn$	$C_{24}H_{32}N_2OZn$	$C_{22}H_{34}N_4OZn$
formula weight	294.68	429.89	435.90
temp (K)	168(2)	203(2)	168(2)
space group	monoclinic *P*2(1)/*n*	monoclinic *P*2(1)/*n*	monoclinic *P*2(1)/*n*
a (Å)	8.628(9)	8.9458(11)	8.8842(14)
b (Å)	11.750(12)	17.864(2)	16.646(3)
c (Å)	14.070(14)	14.3718(17)	15.350(2)
β (deg)	94.259(18)	94.455(2)	96.162(3)
V(Å^3)	1422(3)	2289.7(5)	2256.9(6)
Z	4	4	4
D_{calcd} (Mg/m^3)	1.376	1.247	1.283
μ (Mo Kα) (mm^{-1})	1.714	1.088	1.107
R1[a] (%) (all data)	8.35 (12.30)	2.99 (3.45)	4.29 (6.20)
wR2[b] (%) (all data)	20.25 (21.72)	7.55 (7.82)	8.36 (8.94)

[a] $R1 = \sum||F_o| - |F_c||/\sum|F_o| \times 100$. [b] $wR2 = [\sum w(F_o^2 - F_c^2)^2/\sum(w|F_o|^2)^2]^{1/2} \times 100$.

Table 4. Data Collection Parameters for 9 and 9a

	compound	
	9	**9a**
chemical formula	$C_{26}H_{36}N_2OZn$	$C_{32}H_{52}O_2Zn_2$
formula weight	457.94	599.48
temp (K)	168(2)	168(2)
space group	monoclinic *P*2(1)/*c*	monoclinic *P*2(1)/*n*
a (Å)	11.177(4)	10.1258(14)
b (Å)	21.960(7)	9.8195(14)
c (Å)	20.531(7)	15.366(2)
β (deg)	99.108(5)	92.717(3)
V (Å^3)	4976(3)	1526.1(4)
Z	8	2
D_{calcd} (Mg/m^3)	1.223	1.305
μ (Mo Kα) (mm^{-1})	1.005	1.597
R1[a] (%) (all data)	7.14 (13.65)	4.08 (5.95)
wR2[b] (%) (all data)	11.21 (13.22)	8.62 (9.28)

[a] $R1 = \sum||F_o| - |F_c||/\sum|F_o| \times 100$. [b] $wR2 = [\sum w(F_o^2 - F_c^2)^2/\sum(w|F_o|^2)^2]^{1/2} \times 100$.

Table 5. Data Collection Parameters for 10, 10a, and 10b

	compound		
	10	**10a**	**10b**
chemical formula	$C_{26}H_{28}N_2O_2Zn$	$C_{24}H_{30}N_4O_2Zn$	$C_{25}H_{29}N_3O_2Zn$
formula weight	465.87	471.89	468.88
temp (K)	168(2)	168(2)	168(2)
space group	monoclinic *C*2/*c*	monoclinic *C*2/*c*	orthorhombic *P*2(1)2(1)2(1)
a (Å)	14.232(3)	13.972(3)	12.862(2)
b (Å)	12.391(3)	12.312(2)	13.097(3)
c (Å)	14.194(3)	14.233(3)	14.012(3)
β (deg)	108.743(4)	106.487(4)	
V (Å^3)	2370.5(10)	2347.6(8)	2360.4(7)
Z	4	4	4
D_{calcd} (Mg/m^3)	1.305	1.335	1.319
μ (Mo Kα) (mm^{-1})	1.060	1.073	1.066
R1[a] (%) (all data)	2.94 (3.53)	4.56 (6.36)	4.64 (5.69)
wR2[b] (%) (all data)	6.93 (7.15)	8.82 (9.40)	10.71 (11.18)

[a] $R1 = \sum||F_o| - |F_c||/\sum|F_o| \times 100$. [b] $wR2 = [\sum w(F_o^2 - F_c^2)^2/\sum(w|F_o|^2)^2]^{1/2} \times 100$.

factors. Additionally, the use of bond length restraints was employed to facilitate refinement stability. All C−C bonds were restrained to be equal ($\sigma = 0.04$ Å). Also, all C−O bonds were restrained to be equivalent ($\sigma = 0.04$ Å).

Results and Discussion

While zinc-containing species have been widely reported,[3,5] there is a dearth of structural information on ethyl alkoxy zinc species. This is especially surprising since $ZnEt_2$ is commercially available and widely used.

Table 6. Data Collection Parameters for 11, 11a, 12, and 12a

	compound			
	11	**11a**	**12**	**12a**
chemical formula	$C_{34}H_{44}N_2O_2Zn$	$C_{152}H_{220}N_{16}O_{10}Zn_4$	$C_{40.5}H_{54.5}N_{2.5}O_2Zn$	$C_{38.5}H_{56.5}N_{4.5}O_2Zn$
formula weight	578.08	2692.92	673.74	679.75
temp (K)	168(2)	168(2)	168(2)	168(2)
space group	monoclinic $C2/c$	triclinic $P(\bar{1})$	triclinic $P(\bar{1})$	triclinic $P(\bar{1})$
a (Å)	15.573(5)	19.631(3)	9.730(13)	9.9659(15)
b (Å)	10.764(3)	19.768(3)	11.7125(15)	11.3618(17)
c (Å)	19.106(6)	21.383(4)	16.829(2)	17.525(3)
α (deg)		91.914(3)	102.641(2)	73.833(3)
β (deg)	101.762(5)	93.064(3)	99.233(2)	87.377(3)
γ (deg)		114.479(3)	90.565(2)	87.482(3)
V (Å^3)	3137(3)	7527(2)	1846.8(4)	1902.9(5)
Z	4	2	2	2
D_{calcd} (Mg/m^3)	1.225	1.188	1.212	1.186
μ (Mo Kα) (mm^{-1})	0.814	0.690	0.701	0.682
R1[a] (%) (all data)	3.38 (4.34)	4.05 (5.79)	3.54 (4.63)	3.53 (4.18)
wR2[b] (%) (all data)	7.89 (8.47)	10.23 (10.88)	8.01 (8.35)	8.82 (9.08)

[a] $R1 = \sum||F_o| - |F_c||/\sum|F_o| \times 100$. [b] $wR2 = [\sum w(F_o^2 - F_c^2)^2/\sum(w|F_o|^2)^2]^{1/2} \times 100$.

Table 7. Data Collection Parameters for 13

compound	**13**
chemical formula	$C_{28}H_{56}O_8Zn_4$
formula weight	782.21
temp (K)	168(2)
space group	tetragonal $I4(1)/a$
a (Å)	17.491(5)
b (Å)	17.491(5)
c (Å)	11.197(4)
V (Å^3)	3425.7(17)
Z	4
D_{calcd} (Mg/m^3)	1.517
μ (Mo Kα) (mm^{-1})	2.809
R1[a] (%) (all data)	8.68 (10.62)
wR2[b] (%) (all data)	22.91 (25.27)

[a] $R1 = \sum||F_o| - |F_c||/\sum|F_o| \times 100$. [b] $wR2 = [\sum w(F_o^2 - F_c^2)^2/\sum(w|F_o|^2)^2]^{1/2} \times 100$.

In the literature, there is only one simple alkyl Zn{[Zn(μ_3−OMe)(Et)]$_3$}$_2$[11] and one aryl [Zn(Et)(DBP)]$_2$[12,13] structurally characterized species reported. A number of polydentate complex ligated species have been characterized, including calixarenes,[14] polyphenolates,[15,16] polyacetate,[17] and amylalcohlate.[18−20] However, there is a significant void of structurally diverse alkoxy alkyl derivatives of Zn available.

We were interested in these species as precursors to ZnO nanoparticles since the alkyl moiety will allow for rapid decomposition and the alkoxide ligand will introduce the oxide. Therefore, we undertook the synthesis and characterization of this novel family of compounds and used their diverse structures to synthesize ZnO nanoparticles. The details of this investigation are discussed below.

Synthesis. The synthesis of a variety of "Zn(OR)(Et)(solv)" and "Zn(OR)$_2$(solv)$_2$" were realized through the reaction of the $ZnEt_2$ and the appropriate HOR. The stoichiometry of the reaction dictates the ligand distribution (eq 1). The reaction is very exothermic with rapid bubbling upon mixing of the two reagents. For a select few $n = 1$ stoichiometric reactions, there is a slight yellowing of the reaction mixture, with the remaining solutions being clear and colorless. For $n = 2$, unless sterically hindering ligands coupled with strong Lewis bases are used, the reaction mixture forms a precipitate that is not soluble in noncoordinating solvents (i.e., hexanes, toluene, etc.). The hetero-ligated species are much more soluble than the homoleptic species presumably due to a reduction in oligomerization based on the fact that alkyl ligands typically do not bridge between two metal centers. The homoleptic aryloxides were the most soluble of this subset of compounds due to the increased steric bulk of the aryloxide ligands.

$$ZnEt_2 + nHOR \rightarrow ZnEt_{2-n}(OR)_n \quad n = 1, 2 \qquad (1)$$

The FT-IR spectra of **1**−**13** exhibit no stretches associated with −OH ligands, indicative of complete substitution by the alcohol-alkyl exchange (eq 1). The standard alkyl and aryl stretches for the aryloxide as well as ethyl stretches are present in each sample with small variations based upon the ligand substitution. Due to the complexity of the M−O region, it was not possible to definitively assign a Zn−O stretch.

For the bulk powders of the nonsolvated species elemental analyses are consistent with their respective crystal structures. We have noted that solvated species give inconsistent results due to preferential loss of the solvent or additional residual solvent present due to low volatility of these Lewis bases.[21−23] In addition, we

(11) Ishimori, M.; Hagiwara, T.; T., T.; Kai, Y.; Yasukoa, N.; Kasai, N. *Bull. Chem. Soc. Jpn.* **1976**, *49*, 1165.
(12) Parvez, M.; Bergstreser, G.; Richey, H. G. *ACA Abstr. Pap. (Winter)* **1986**, *14*, 28.
(13) Parvez, M.; Bergstresser, G. L.; Richey, H. G. *Acta Crystallogr., Sect. C: Cryst. Struct. Commun.* **1992**, *48*, 641.
(14) Gardiner, M. G.; Lawrence, S. M.; Raston, C. L.; Skelton, B. W.; White, A. H. *Chem. Commun.* **1996**, 2491.
(15) Dinger, M. B.; Scott, M. J. *Inorg. Chem.* **2001**, *40*, 1029.
(16) Chisholm, M. H.; Lin, C.-C.; Gallucci, J. C.; Ko, B.-T. *Dalton Trans.* **2003**, 406.
(17) Dekker, J.; Schouten, A.; Budzelaar, P. H. M.; Boersma, J.; Vanderkerk, G. J. M.; Spek, A. L.; Duisenber, A. J. M. *J. Organomet. Chem.* **1987**, *320*, 1.
(18) Bolm, C.; Schlingloff, G.; Harms, K. *Chem. Ber.* **1992**, *125*, 1.
(19) Steinborn, D.; Rausch, M.; Baumeister, W.; Potocnak, I.; Miklos, D.; Dunaj-jurco, M. *Z. Anorg. Allg. Chem.* **1996**, *622*, 1941.
(20) Mimoun, H.; De Saint Laumer, J. Y.; Giannini, L.; Scopelliti, R.; Floriani, C. *J. Am. Chem. Soc.* **1999**, *121*, 6158.
(21) Boyle, T. J.; Alam, T. M.; Peters, K. P.; Rodriguez, M. A. *Inorg. Chem.* **2002**, *40*, 6281.
(22) Boyle, T. J.; Andrews, N. L.; Rodriguez, M. A.; Campana, C.; Yiu, T. *Inorg. Chem.* **2003**, *42*, 5357.
(23) Boyle, T. J.; Pedrotty, D. M.; Alam, T. M.; Vick, S. C.; Rodriguez, M. A. *Inorg. Chem.* **2000**, *39*, 5133.

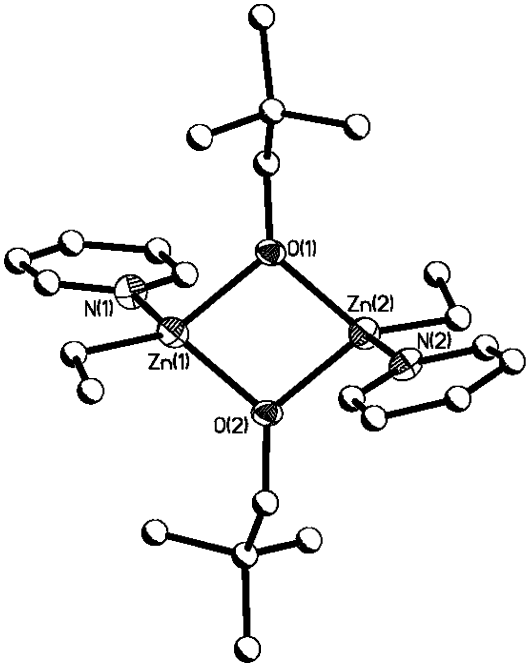

Figure 2. Thermal ellipsoid plot of **1**. Ellipsoids are drawn at the 30% level.

attempted to remove residual py or MeIm through washes with organic solvents; however, these attempts may have also removed bound solvent, complicating the identity of the bulk powder. Therefore, the elemental analyses of the isolated species do not necessarily correspond to the molecular formula calculated from their crystal structures.

X-ray Crystallographic Structures. Due to the lack of systematic studies on $Zn(Et)_{2-x}(OR)_x$ structures discussed previously, we undertook the crystallographic identification of this novel family of precursors. Structural modifications focused on the substitution of the Et groups with the alcohols (eq 1) shown in Figure 1. Data collection parameters are shown in Tables 1−7.

Based on our previous success with ONep ligands,[21,24−28] we initiated our exploration of Zn precursors with this ligand. The structure isolated for $n = 1$ (eq 1) proved to be a solvated dinuclear species (**1**) wherein each Zn was tetrahedrally (T_d) bound by two μ-ONep, one terminal Et, and one py ligand. Figure 2 shows the thermal ellipsoid plot of **1**. When the steric bulk of the pendant chain to OBu^t was increased but py was maintained as the solvent, compound **2** was isolated in an identical structure (see Figure 3). Rerunning the reaction of **1** in a non-Lewis basic solvent led to the isolation of a cube structure, **3**, shown in Figure 4. Each Zn is again in a T_d geometry using three μ_3-ONep and one Et terminal ligand to fill its coordination sphere.

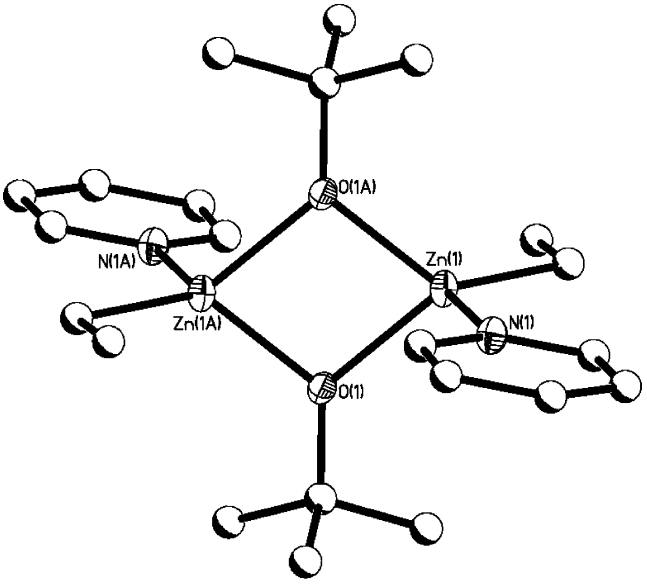

Figure 3. Thermal ellipsoid plot of **2**. Ellipsoids are drawn at the 30% level.

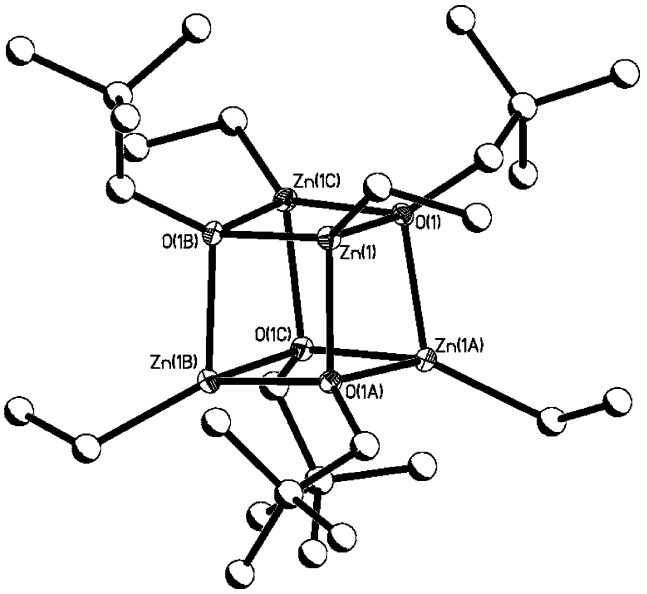

Figure 4. Thermal ellipsoid plot of **3**. Ellipsoids are drawn at the 30% level.

When the shape of the pendant hydrocarbon chain is altered, the amount of steric bulk around the Zn metal center is also varied, which can play a vital role in final structural arrangements. Therefore, with use of the $H-OCH_2Pr^c$ (Figure 1c) modifier, an unusual heptanuclear species **4** was isolated. Figure 5 shows the thermal ellipsoid plot of **4**. This molecule consists of two point shared Zn−O cubes. Six of the Zn atoms were T_d coordinated with the shared Zn adopting an octahedral (O_h) geometry. For the T_d-bound Zn atoms three μ_3-OCH_2Pr^c and one terminal Et ligand fill the metal centers geometry, whereas for the O_h-bound Zn only μ_3-OCH_2Pr^c ligands are used. Increasing the ring size by one (Figure 1d) or by two (Figure 1e) led to the isolation of **5** and **6**, respectively. Figures 6 and 7 show the thermal ellipsoid plot of **5** and **6**, respectively. Each of these compounds adopts a cube structure similar to what was noted for **3**. The increased steric bulk of these ligands must account for the tetranuclear versus hep-

(24) Boyle, T. J.; Alam, T. M.; Mechenbeir, E. R.; Scott, B.; Ziller, J. W. *Inorg. Chem.* **1997**, *36*, 3293.
(25) Boyle, T. J.; Alam, T. M.; Dimos, D.; Moore, G. J.; Buchheit, C. D.; Al-Shareef, H. N.; Mechenbier, E. R.; Bear, B. R. *Chem. Mater.* **1997**, *9*, 3187.
(26) Boyle, T. J.; Gallegos, J. J., III; Pedrotty, D. M.; Mechenbier, E. R.; Scott, B. L. *J. Coord. Chem.* **1999**, *47*, 155.
(27) Boyle, T. J.; Pedrotty, D. M.; Scott, B.; Ziller, J. W. *Polyhedron* **1997**, *17*, 1959.
(28) Boyle, T. J.; Zechmann, C. A.; Alam, T. M.; Rodriguez, M. A.; Hijar, C. A.; Scott, B. L. *Inorg. Chem.* **2002**, *41*, 946.

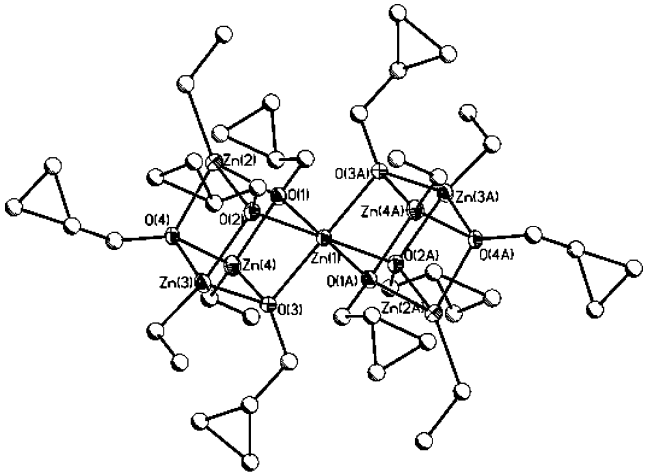

Figure 5. Thermal ellipsoid plot of **4**. Ellipsoids are drawn at the 30% level.

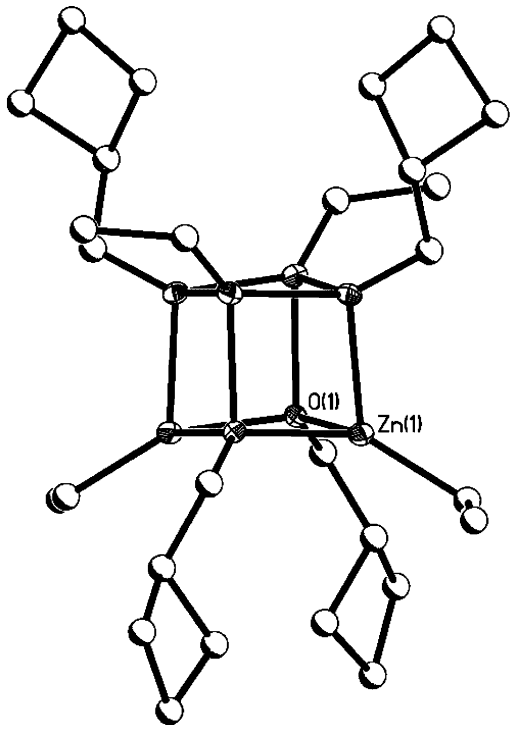

Figure 6. Thermal ellipsoid plot of **5**. Ellipsoids are drawn at the 30% level.

tanuclear species isolated for **5** and **6** versus **3**, respectively.

Introducing aryloxide ligands yields dinuclear species similar to **1**. For the DMP (Figure 1g) derivative **7**, the aryloxide acts as a bridging ligand with a terminal Et and bound py molecule forming a T_d Zn metal center. When the steric bulk in the ortho position is increased to an *iso*-propyl (DIP, Figure 1h) or *tert*-butyl (DBP, Figure 1i), a monomer forms: **8** or **9** (py) or **8a**. Removal of the Lewis basic solvent for the DBP led to the formation of dimeric species **9a**. Switching to the homoleptic aryloxide ligands also led to the isolation of solvated monomeric species. For py (**10**, **11**, and **12**) or MeIm (**10a**, **11a**, and **12a**) solvated species, each Zn metal center was T_d bound by the requisite OAr and the coordination of two solvent molecules. A mixed solvent species was also isolated (**10b**). Due to the similarity of structures, selected compounds are shown.

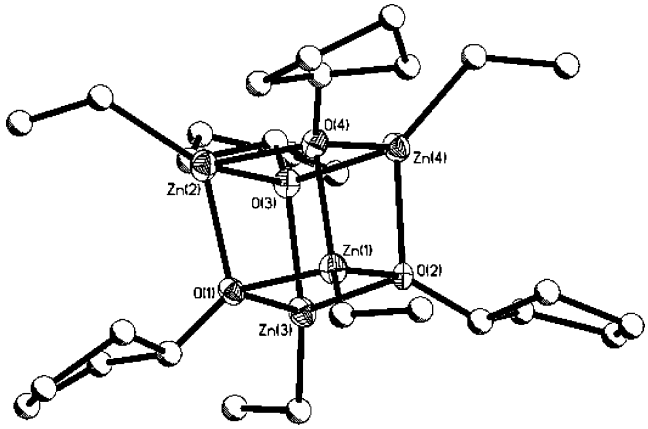

Figure 7. Thermal ellipsoid plot of **6**. Ellipsoids are drawn at the 30% level.

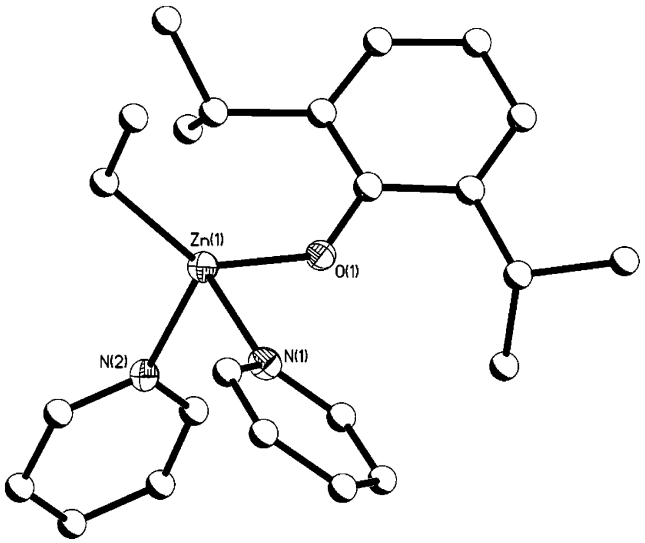

Figure 8. Thermal ellipsoid plot of **8**. Ellipsoids are drawn at the 30% level.

Figures 8 and 9 show the thermal ellipsoid plots of **8** and **9a**, respectively.

We have also investigated the use of bidentate ligands in generating these mixed ligated Zn species. One of interest is the H−OTHF (Figure 1f) ligand. The structure isolated for **13** was a cube (Figure 10) as noted for **3**, **4**, and **6**. The coordination of the Zn metal center is sufficiently filled without requiring the additional Lewis basic oxygen from the THF moiety.

Solution NMR. Crystalline material of each sample was redissolved in the appropriate deuterated solvent, except for MeIm, wherein py-d_5 was used to solubilize the compounds. For the ONep, OBu^t, and aryl oxide derivatives little information was garnered concerning the solution behavior from these experiments since only the resonances associated with the pendant aryl chains were observed. However, all the solvated aryloxide derivatives are monomeric and it is assumed they remain so in their parent solution. The dinuclear and cube structures show simple NMR spectra indicative of the high symmetry of the crystalline material.

The solution behavior of **4**, a heptanuclear complex in the solid state, was investigated in benzene-d_6. For this complex, the ^{1}H NMR spectra revealed two sets of cyclopropyl methoxide resonances with an integration ratio of 3:1 and one set of resonances that correspond

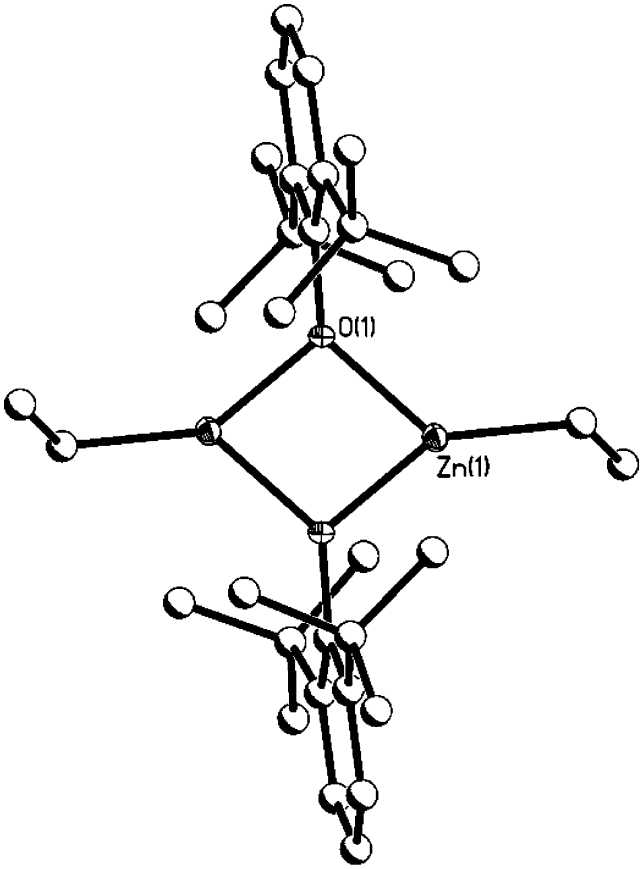

Figure 9. Thermal ellipsoid plot of **9a**. Ellipsoids are drawn at the 30% level.

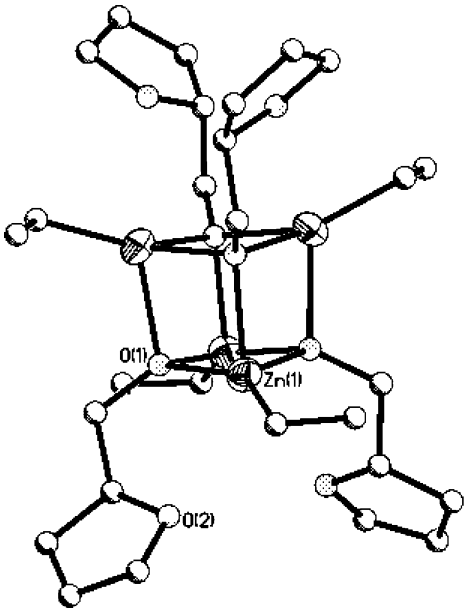

Figure 10. Thermal ellipsoid plot of **13**. Ellipsoids are drawn at the 30% level.

to six equivalent ethyl ligands. It can therefore be inferred that the structure of the heptanuclear complex, similar to the previously discussed dinuclear and tetranuclear structures, remained intact in solution.

Nanoparticles. Selected species (**8**, **1**, **13**, and **4**) representing the various nuclearities (mono-, di-, tetra-, and heptanuclear) noted for the family of "Zn(OR)(Et)(solv)" were chosen to investigate the effect of precursor nuclearity on the final morphology of nanoparticles. The concept of using molecular clusters as growth nuclei for nanoparticles has been previously explored[29,30] but our study focuses on the structural variations of the precursor and how they affect final morphologies of the nanoparticles. Several reports have used molecular precursors, such as $[(Me)Zn(OSiMe_3)]_4$[31] and "$EtZn(OCHMe_2)$",[32] for the production of ZnO. The syntheses reported in these studies are different from the one presented in this work. Due to large variations that can occur in the final morphology from subtle changes in the synthesis conditions, a comparison between final morphologies for these systems and the one presented here is difficult. Table 8 is a summary of structure types and morphology generated in this method.

Table 8. Summary of Precursors' Nuclearity and Final ZnO Morphologies

compound	nuclearity	representative compound	nanoparticle morphology
7−**12**	mono	**8**	spheroids (>10 nm)
1, **2**	di	**1**	rods (50 × 7.5 nm)
3, **5**, **6**, **13**	tetra	**13**	rods (95 × 10 nm)
4	hepta	**4**	rods (50 × 13 nm)

For this work, each compound was redissolved in pyridine and injected into a refluxing mixture of MeIm and water mixture (95:5). In theory, the water would hydrolyze the particles and the MeIm would act as both the solvent and surfactant, preventing larger particles from forming. This was previously employed to successfully generate nanoparticles of $Co(OH)_2$.[33] After the appropriate workup, the powder was analyzed by XRD and found to be the wurtzite structure of ZnO.

With use of compound **8**, the TEM images of the resultant nanoparticles shown in Figure 11a were obtained. The particles are irregular spheroids with an average diameter >10 nm in size. Switching to the dinuclear species **1**, very distinct and uniform rods are formed (Figure 11b). The rods have the dimensions of ∼50 × 7.5 nm. Similarly, the materials formed by **13** also yield long thin rods of dimensions slightly larger with some of the more distinct rods having dimensions of ∼95 × 10 nm. The heptanuclear species **4** also forms rods; however, these are much more rounded with dimensions of ∼50 × 13 nm. Clearly, the wurtzite structure of ZnO favors the growth of rodlike materials;[34−38] however, subtle influences by either the ligands or nuclearity greatly affect the final morphology. All of the ligands are alkoxides with similar decomposition pathways; therefore, a great deal of the observed dif-

(29) Cumberland, S. L.; Hanif, K. M.; Javier, A.; Khitrov, G. A.; Strouse, G. F.; Woessner, S. M.; Yun, C. S. *Chem. Mater.* **2002**, *14*, 1576.
(30) Monge, M.; Kahn, M. L.; Maisonnat, A.; Chaudret, B. *Angew. Chem.* **2003**, *42*, 5321.
(31) Hambrock, J.; Rabe, S.; Merz, K.; Birkner, A.; Wohlfart, A.; Fisher, R. A.; Driess, M. *J. Mater. Chem.* **2003**, *13*, 1731.
(32) Kim, C. G.; Sung, K.; Chung, T.-M.; Jung, D. Y.; Kim, Y. *Chem. Commun.* **2003**, 2068.
(33) Boyle, T. J.; Rodriguez, M. A.; Ingersoll, D.; J. H. T.; Bunge, S. D.; Pedrotty, D. M.; De'Angeli, S. M.; Vick, S. C.; Fan, H.-Y. *Chem. Mater.* **2002**, *15*, 3903.
(34) Guo, M.; Diao, P.; Cai, S. M. *Acta Chim. Sin.* **2003**, *61*, 1165.
(35) Tseng, Y. K.; Lin, I. N.; Liu, K. S.; Lin, T. S.; Chen, I. C. *J. Mater. Res.* **2003**, *18*, 714.
(36) Lao, J. Y.; Huang, J. Y.; Wang, D. Z.; Ren, Z. F. *Nano Lett.* **2003**, *3*, 235.
(37) Guo, L.; Ji, Y. L.; Xu, H. B.; Simon, P.; Wu, Z. Y. *J. Am. Chem. Soc.* **2002**, *124*, 14864.
(38) Xu, C. X.; Sun, X. W. *Jpn. J. Appl. Phys. Part 1* **2003**, *42*, 4949.

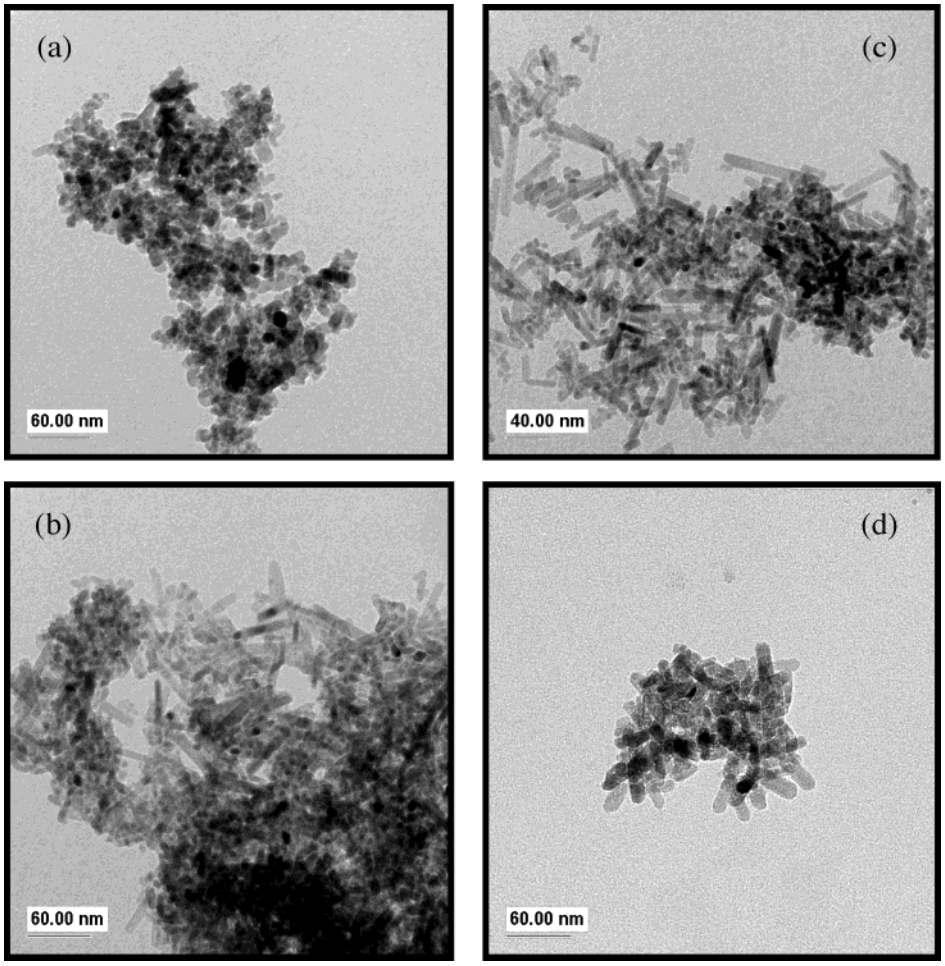

Figure 11. TEM images of ZnO nanoparticles generated from a solution of (a) **8**, (b) **1**, (c) **13**, or (d) **4** injected into hot MeIm/H_2O (95:5).

ferences in the final nanorod dimensions must be attributed to the nuclearity of the starting materials.

Wurtzite adopts a hexagonal unit cell ($P63mc$, $Z = 2$) with $a = 3.249$ Å and $c = 5.205$ Å with every tetrahedrally coordinated Zn and O atoms oriented in one direction. The overall structure therefore consists of Zn and O atoms stacked in a layered AB/AB/AB hexagonal sequence. Figure 12 shows a schematic of the structure and a packing diagram. As can be seen, there are four atoms per unit cell that when extended reveals a complex structure that consists of a chain of three distorted fused six-membered rings. With use of the central core of the structurally characterized precursors as the basic building blocks to the resultant ZnO nanorods, an explanation for the variations of the final nanorods isolated can be proffered.

For all the precursors, the central core composed of Zn and O atoms will be considered the building block to the rods formed since the removal of hydrocarbons would be the first step in the decomposition of these precursors under the conditions investigated. This would yield a square, a cube, and point-joined cube (**1**, **13**, and **4**), respectively, as the basic building block. The calculated volumes for the compounds of **1**, **13**, and **4** were found to be ~2822, 9500, and 8450 Å^3, respectively, with aspect ratios of the resultant nanorods from the same precursors calculated as 6.67, 9.50, and 3.84.

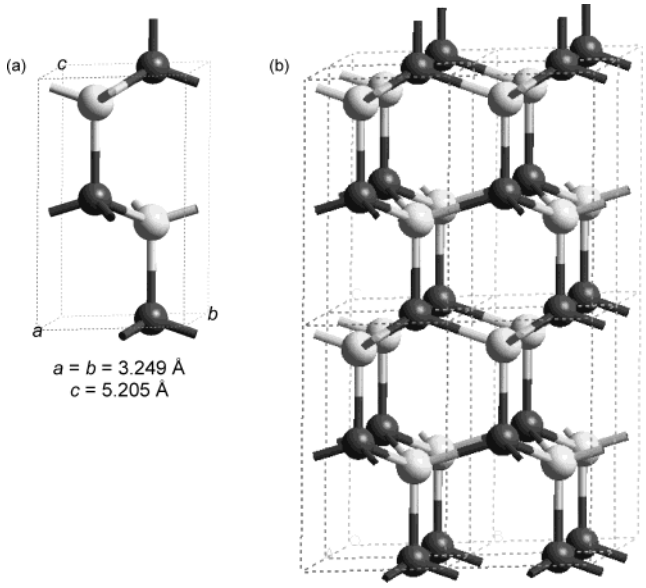

Figure 12. Schematic representation of wurtzite (a) unit cell and (b) 2 × 2 × 2 unit cell moiety. Zn atoms (black spheres) and O atoms (gray spheres).

To have the dinuclear or square shape form the wurtzite structure, the squares must properly align and then break a single Zn−O bond, linking up as shown in Figure 13a. Obviously, there are numerous directions in which the dinuclear Zn−O species can link; however,

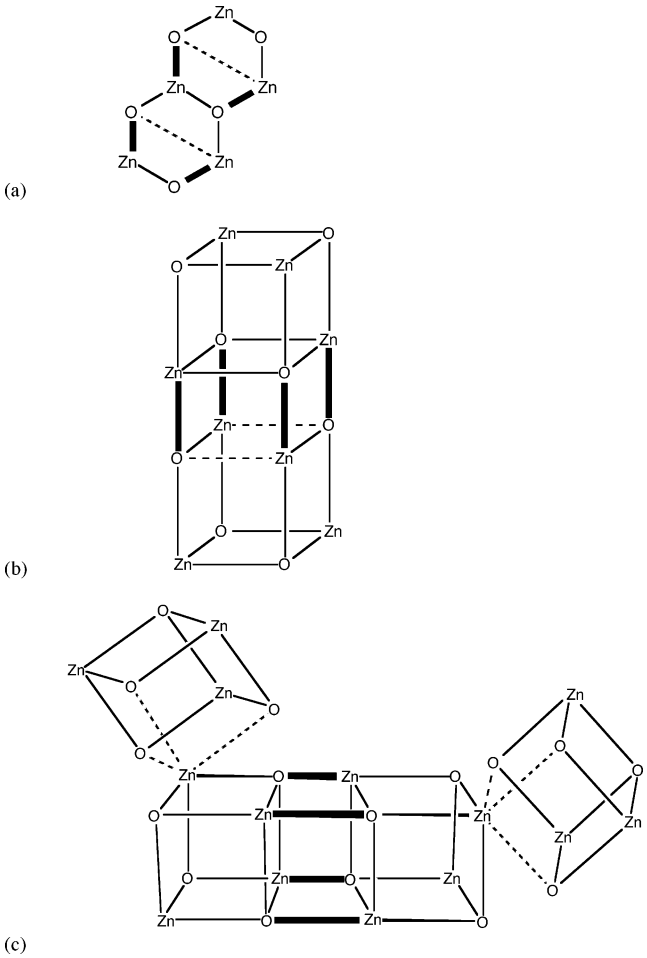

Figure 13. Schematic of idealized building blocks from molecules (a) **1**, (b) **13**, and (c) **4**. The dashed lines represent bonds broken from the original molecule and bold lines represent new bonds formed.

once a growth plane has been established, some statistical growth patterns will emerge. For the square precursors, it is not unreasonable to expect the edges to grow faster that the faces since only two atoms must align versus lateral growth wherein four atoms must align. However, it is important to note that simple rotations can correct any misalignment. Therefore, growth in one direction may be *slightly* more favored than the other, which is consistent with the observed aspect ratios.

For the cube, once any two cubes are bound (Figure 13b), statistically growth in the longer direction will be favored. For terminal growth, the cube only has to match one face, which can be easily accomplished by simple rotation; however, for lateral growth the first cube again only has to match the initial face but subsequent cubes must match at a minimum two faces, which will be statistically less favored. Therefore, growth will occur preferentially in one direction and in a more pronounced manner than noted for the cube. This is consistent with the observed aspect ratios of the nanorods formed.

As observed in Figure 13c, similar rod structures can be formed by linking cube moieties of the central core of **13**. However, the pendant cube of **13** may sterically prevent further growth in that direction. There is an additional open coordination site on the newly formed cube that could allow for growth in the opposite direction. At some point, growth in all directions will be hindered by the steric bulk of the pendant cube. To form the wurtzite phase, the six-coordinated Zn must transform to a T_d geometry by loss of the pendant cube moiety (see Figure 13c). Therefore, this moiety must break up, which can occur by several mechanisms and will lead to random growth. Thus, one would expect potential rods forming but both growth directions can occur, which would be consistent with the observed aspect ratios. The volume of the rods formed from **4** in comparison to those isolated for **13** are similar, which would be consistent with the cube growth process.

Summary and Conclusion

We have successfully synthesized and characterized a novel family of structurally varied Zn heteroleptic (alkyl alkoxides) and homoleptic (alkoxide) compounds (**1**−**13**). Four representative nuclearities, mono- (**8**), di- (**1**), tetra- (**13**), and hepta- (**4**) nuclear were selected as precursors to nanoparticles. All of these compounds were successfully used to generate ZnO nanomaterials. For the mononuclear species spherically shaped nanoparticles were observed. As the nuclearity increased, rods were formed with aspect ratios 6.67 for the dinuclear species **1** and 9.5 for the cube **13**. Switching to the point-joined cube, heptamer (**4**) yielded a smaller aspect ratio of 3.84. Due to the similarity of the morphologies of all particles generated, wurtzite preferentially grows in a rodlike morphology; however, the precursors investigated here were shown to have an effect on the shape and dimensions of these rods. More work on structurally varied precursors is necessary to further establish this concept; however, from this novel family of precursors under the conditions investigated (MeIm/H_2O reflux temperatures), it is proposed that the central core building blocks have an effect on the constructs of the nanorods. A cube structure was found to yield the thinnest rods and the sterically hindering heptamer yields thicker rods. Further work to control the growth of these rods through variations in the precursor structure is underway.

Acknowledgment. For support of this research, the authors would like to thank the Office of Basic Energy Science of the Department of Energy and the United States Department of Energy. The authors would also like to acknowledge Ms. Irma M. Saechao for technical assistance and Dr. R. T. Cygan (SNL) for computational model figures. Sandia is a multiprogram laboratory operated by Sandia Corporation, a Lockheed Martin Company, for the United States Department of Energy under Contract DE-AC04-94AL85000.

Supporting Information Available: X-ray crystallographic files in CIF format for the structures **1**−**13** and additional information concerning the data collection and final structural solutions of **1**−**13** in PDF format. This material is available free of charge via the Internet at http://pubs.acs.org. The X-ray crystallographic files for structures **1**−**13** are also available from the Cambridge Data Base.

CM0493997